

Quantum Frenkel-Kontorova Model

Bambi Hu

Department of Physics and Centre for Nonlinear Studies, Hong Kong Baptist University, Hong Kong, China

Department of Physics, University of Houston, Houston, TX 77204-5506, USA

Baowen Li

Department of Physics and the Centre for Nonlinear Studies, Hong Kong Baptist University, Hong Kong, China

Department of Physics, National University of Singapore, 119260 Singapore

Abstract

This paper gives a review of our recent work on the quantum Frenkel-Kontorova model. Using the squeezed state theory and the quantum Monte Carlo method, we have studied the effects of quantum fluctuations on the Aubry transition and the behavior of the ground state wave function. We found that quantum fluctuations renormalize the sinusoidal standard map to a sawtooth map. Although quantum fluctuations have smeared the Aubry transition, the remnants of this transition are still discernible. The ground state wave function also changes from an extended state to a localized state. The squeezed state results agree very well with those from the Monte Carlo and mean field studies.

Key words: Frenkel-Kontorova model; squeezed state; quantum phase transitions; quantum chaos

PACS: 64.70.Rh, 64.70.-p, 5.45.+Jn, 42.50.Dv

1 Introduction

Many physical systems such as charge density waves, magnetic spirals, Josephson junctions and adsorbed monolayers exhibit a competition between two or more length scales. To understand such modulated structures, a simple model, known as the Frenkel-Kontorova (FK) model [1], was introduced more than half a century ago. The FK model describes a chain of atoms connected by springs in the presence of an external sinusoidal potential. It has two length scales: the natural length of the spring and the period of the external potential.

Due to the competition between these two length scales, the FK model exhibits a wealth of interesting and complex phenomena. Extensive studies of the FK model have been made since its introduction. In most of the earlier studies, the FK model was treated in the continuum approximation. Although the continuum approximation, which reproduces the sine-Gordon equation and its soliton solutions, gives some very useful information, it misses many essential features. A major advance in the study of the FK model was made by Aubry [2]. Aubry reverted to the discrete version of the FK model and made essential use of the seminal Kolmogorov-Arnol'd-Moser (KAM) theorem. In analogy to the breakup of a KAM torus, Aubry discovered the “transition by breaking of analyticity.” The Aubry transition is similar to a phase transition, thus all the apparatus invented in the study of second-order phase transitions can be borrowed to study this transition. A fairly complete picture of the FK model was thus obtained.

So far most of the studies made on the FK model have been confined to the classical model. Very little study has been done on the quantum FK model. Although the FK model looks simple, it's nevertheless a non-integrable interacting many-body system. There aren't that many methods at our disposal to study the quantum behavior of such a model. Moreover, besides theoretical interest, there are also practical considerations that demand a deeper understanding of the quantum FK model. For example, the study of friction, or tribology [3], is a very important subject both in terms of fundamental science and applications. And indeed, the FK model has been used to study tribology. However, as technology is moving into the nano-regime, nanotribology [4] is also becoming a very important subject of study. In the nano-regime, it's more likely than not that quantum mechanics will play an important role. This makes an understanding of the quantum FK model not only desirable but very likely imperative. This is the motivation for our interest in the quantum FK model.

The first study of the quantum FK model was made by Borgonovi, Guarneri and Shepelyansky [5]. They mainly used a numerical approach. Later, Berman, Bulgakov and Campbell [6] studied the same problem using a mean-field approach. In our study we will use a hybrid analytical and numerical approach. The analytical method is based on the squeezed state theory, and the numerical method is based on the quantum Monte Carlo (QMC) algorithm.

This paper gives a review of our recent work on the quantum FK model [7,8]. It is organized as follows. In Sec. 2, we will define the quantum Frenkel-Kontorova model and use the Monte-Carlo method to study it. In Sec. 3 we will formulate the squeezed state approach. In Sec. 4 we will study the quantum effects on the Aubry transition. In Sec. 5 some concluding remarks will be given.

2 Quantum Frenkel-Kontorova model

The Hamiltonian of the quantum Frenkel-Kontorova model is described by:

$$\hat{\mathcal{H}} = \sum_i \left[\frac{\hat{p}_i^2}{2m} + \frac{\gamma}{2} (\hat{x}_{i+1} - \hat{x}_i - a)^2 - V \cos(q_0 \hat{x}_i) \right]. \quad (1)$$

Here m is the mass of the particles, γ the elastic constant of the spring, $2\pi/q_0$ the period of the external potential, V the magnitude of the external potential, and a the equilibrium distance between two nearest neighbor particles. For convenience, we shall rescale the variables so as to obtain a dimensionless Hamiltonian

$$\hat{H} = \sum_i \left[\frac{\hat{P}_i^2}{2} + \frac{1}{2} (\hat{X}_{i+1} - \hat{X}_i - \mu)^2 - K \cos \hat{X}_i \right], \quad (2)$$

where $\hat{X}_i = q_0 \hat{x}_i$, $\hat{P}_i = (\frac{q_0}{\sqrt{m\gamma}}) \hat{p}_i$, $\mu = q_0 a$, and $K = V q_0^2 / \gamma$. We define an “effective Planck’s constant”:

$$\tilde{\hbar} = \left(\frac{q_0^2}{\sqrt{m\gamma}} \right) \hbar. \quad (3)$$

This effective Planck’s constant is the ratio of the natural quantum energy scale $\hbar\omega_0$ to the natural classical energy scale γ/q_0^2 , and $\omega_0^2 = \gamma/m$. This quantity provides a measure of the importance of quantum effects. In particular, quantum effects become crucial at zero temperature when thermal fluctuations vanish.

In the classical FK model, the positions of the particles in the ground state, denoted by X_i^e , are determined by the following equation:

$$X_{i+1}^e - 2X_i^e + X_{i-1}^e = K \sin X_i^e. \quad (4)$$

This equation can be cast into the form of the standard map by defining $I_{i+1} = X_{i+1}^e - X_i^e$:

$$\begin{aligned} I_{i+1} &= I_i + K \sin X_i^e, \\ X_{i+1}^e &= I_{i+1} + X_i^e. \end{aligned} \quad (5)$$

To describe the transition from the unpinned phase in the subcritical regime to the pinned phase in the supercritical regime, the hull function is introduced.

It is defined by

$$X_i^e = f(X_i). \quad (6)$$

Here X_i is the unperturbed ($K = 0$) particle position. Another useful function is called the g -function, defined by

$$g = \frac{1}{K}(X_{i+1}^e - 2X_i^e + X_{i-1}^e) \quad (7)$$

For $K < K_c$, the ground state of the classical FK model corresponds to an invariant curve in the standard map (5). The hull function is a monotonic analytical function [Fig. 1(a)], and the g -function is $g(X) = \sin X$ [Fig. 1(b)]. At $K = K_c$, the last invariant curve in the standard map breaks up and becomes a Cantorus. The hull function becomes a monotonic function with a countable number of discontinuities [Fig. 1(c)], and the g -function becomes a Cantor subset of the function $\sin X$ [Fig. 1(d)].

By using the quantum Monte Carlo method, we can calculate the ground state averages of the particle positions \bar{X}_i and plot the following three functions so as to compare with their classical counterparts: (1) The quantum hull function, i.e., \bar{X}_i as a function of the unperturbed positions X_i ; (2) the quantum g -function which is defined as

$$g_q = \frac{1}{K}(\bar{X}_{i+1} - 2\bar{X}_i + \bar{X}_{i-1}); \quad (8)$$

and (3) (\bar{X}_i, \bar{I}_i) in the phase space of the standard map.

The quantum effect does not destroy the functional dependence of g_q on \bar{X}_i , instead it renormalizes it to a sawtooth map [Fig. 2]. This phenomenon was first observed by Borgonovi *et al.* [5] and was interpreted as a consequence of quantum tunneling between the edges of the gap in the hull function.

3 Squeezed state approach

In this section, we will study the effect of quantum fluctuations on the FK model by using the squeezed state approach [7].

The squeezed state was first used in quantum optics and has proven to be very useful in many other fields [9–13]. The squeezed state approach starts from

the time-dependent variational principle

$$\delta \int dt \langle \Psi(t) | i\hbar \frac{\partial}{\partial t} - \hat{H} | \Psi(t) \rangle = 0. \quad (9)$$

Variation with respect to (w.r.t.) $\langle \Psi(t) |$ gives rise to the Schrödinger equation. The exact solution may be approximated by restricting the choice of states to a subspace of the full Hilbert space. In the squeezed state approach, the squeezed state is chosen as $|\Psi(t)\rangle$.

The squeezed state $|\Phi(\alpha, \beta)\rangle$ is defined by

$$|\Phi(\alpha, \beta)\rangle = e^{\hat{S}(\alpha)} e^{\hat{T}(\beta)} |0\rangle, \quad (10)$$

where

$$\hat{S}(\alpha) = \sum_i (\alpha_i \hat{a}_i^\dagger - \alpha_i^* \hat{a}_i) \quad (11)$$

is the Weyl's displacement operator, and

$$\hat{T}(\beta) = \frac{1}{2} \sum_{ij} (\hat{a}_i^\dagger \beta_{ij} \hat{a}_j^\dagger - \hat{a}_i \beta_{ij}^* \hat{a}_j). \quad (12)$$

is the squeezed state operator. $\hat{S}^\dagger(\alpha) = -\hat{S}(\alpha)$, $\hat{T}^\dagger(\beta) = -\hat{T}(\beta)$. For brevity, we will use the abbreviation $|\Phi\rangle \equiv |\Phi(\alpha, \beta)\rangle$. If $\beta = 0$, the squeezed state is reduced to the coherent state. However, as we shall see later, the coherent state is not adequate to study quantum fluctuations.

The position and momentum operators for the i th particle are written as

$$\begin{aligned} \hat{X}_i &= \sqrt{\frac{\hbar}{2}} (\hat{a}_i^\dagger + \hat{a}_i), \\ \hat{P}_i &= i\sqrt{\frac{\hbar}{2}} (\hat{a}_i^\dagger - \hat{a}_i). \end{aligned} \quad (13)$$

Here, \hat{a}_i^\dagger and \hat{a}_i are the creation and annihilation operators which satisfy the canonical commutation relations: $[\hat{a}_i, \hat{a}_j^\dagger] = \delta_{ij}$, $[\hat{a}_i, \hat{a}_j] = 0$ and $[\hat{a}_i^\dagger, \hat{a}_j^\dagger] = 0$.

Using $|\Phi\rangle$ as a trial wave function, we can find the expectation values of the position and momentum operators of the i th particle [9]:

$$\begin{aligned} \bar{X}_i &\equiv \langle \Phi | \hat{X}_i | \Phi \rangle = \sqrt{\frac{\hbar}{2}} (\alpha_i^* + \alpha_i), \\ \bar{P}_i &\equiv \langle \Phi | \hat{P}_i | \Phi \rangle = -i\sqrt{\frac{\hbar}{2}} (\alpha_i^* - \alpha_i). \end{aligned} \quad (14)$$

Fluctuations in the position and the momentum are given by

$$\begin{aligned}\Delta X_i^2 &\equiv \langle \Phi | (\hat{X}_i - \bar{X}_i)^2 | \Phi \rangle = \tilde{\hbar} G_{ii}, \\ \Delta P_i^2 &\equiv \langle \Phi | (\hat{P}_i - \bar{P}_i)^2 | \Phi \rangle = \tilde{\hbar} \left(\frac{G_{ii}^{-1}}{4} + 4 \sum_{l,k} \Pi_{il} G_{lk} \Pi_{ki} \right).\end{aligned}\quad (15)$$

The fluctuation covariance between the i th particle and the j th particle is

$$\Delta X_i \Delta X_j \equiv \langle \Phi | (\hat{X}_i - \bar{X}_i)(\hat{X}_j - \bar{X}_j) | \Phi \rangle = \tilde{\hbar} G_{ij}, \quad (16)$$

where

$$\begin{aligned}G_{ij} &= \frac{1}{2}(\cosh^2 \sqrt{\beta\beta^\dagger} + \sinh^2 \sqrt{\beta\beta^\dagger})_{ij} + \frac{1}{2}(M\beta + \beta^\dagger M)_{ij}, \\ \Pi_{ij} &= \frac{i}{4}G_{ij}^{-1}(M\beta - \beta^\dagger M)_{ij},\end{aligned}\quad (17)$$

and,

$$M = \frac{\sinh \sqrt{\beta\beta^\dagger} \cosh \sqrt{\beta\beta^\dagger}}{\sqrt{\beta\beta^\dagger}}. \quad (18)$$

Since β is a symmetric matrix, $G_{ij} = G_{ji}$ and $\Pi_{ij} = \Pi_{ji}$. Using the following relation

$$\langle \Phi | \cos \hat{X}_i | \Phi \rangle = \exp\left(-\frac{\tilde{\hbar}}{2}G_{ii}\right) \cos \bar{X}_i, \quad (19)$$

we obtain the expectation value of the Hamiltonian, $\bar{H} \equiv \langle \Phi | \hat{H} | \Phi \rangle$,

$$\begin{aligned}\bar{H} &= \sum_i \frac{1}{2} \left(\bar{P}_i^2 + \tilde{\hbar} \left(\frac{G_{ii}^{-1}}{4} + 4 \sum_{l,k} \Pi_{il} G_{lk} \Pi_{ki} \right) \right) + \sum_i \frac{1}{2} (\bar{X}_{i+1} - \bar{X}_i - \mu)^2 \\ &\quad + \sum_i \frac{\tilde{\hbar}}{2} (G_{ii} + G_{i+1i+1} - 2G_{i+1i}) - \sum_i K \exp\left(-\frac{\tilde{\hbar}}{2}G_{ii}\right) \cos \bar{X}_i.\end{aligned}\quad (20)$$

The variables \bar{X}_i and \bar{P}_i , and G_{ij} and Π_{ij} form explicitly canonical conjugates [10]. To find the ground state of the quantum FK model, we will use a variational approach in which these four variables are treated as independent

variables. Variation with respect to \bar{P}_i and \bar{X}_i yields, respectively,

$$\begin{aligned}\bar{P}_i &= 0, \\ \bar{X}_{i+1} - 2\bar{X}_i + \bar{X}_{i-1} &= K_i \sin \bar{X}_i,\end{aligned}\tag{21}$$

where

$$K_i = K \exp\left(-\frac{\tilde{\hbar}}{2}G_{ii}\right).\tag{22}$$

This equation determines the expectation value of the particle's position. Unlike its classical counterpart ($\tilde{\hbar} = 0$, $K_i = K$), this equation is coupled to the quantum fluctuation by $\tilde{\hbar}G_{ii}$. Variation w.r.t. Π_{ij} leads to

$$\sum_k G_{ik}\Pi_{kj} = 0.\tag{23}$$

To obtain the equation for G_{ij} , we first take variation w.r.t. G_{ik} and note that

$$\frac{\delta G_{ij}}{\delta G_{kl}} = \delta_{ik}\delta_{jl}.\tag{24}$$

We then multiply both sides of the equation by G_{kj} and sum over k . We then get the closed set of equations for the covariance G_{ij} :

$$(GF)_{ij} = G_{i-1j} + G_{i+1j},\tag{25}$$

where

$$F_{ij} = \left(1 + \frac{K_i}{2} \cos \bar{X}_i\right) \delta_{ij} - \frac{(G^{-2})_{ij}}{8}.\tag{26}$$

This is a set of equations determining the quantum fluctuations of the particles. G is an $N \times N$ symmetric matrix which provides information about fluctuations. Its diagonal elements give the variance of each particle while its off-diagonal elements give the covariance between particles. From this information we can calculate the correlation function of the quantum fluctuations. These equations are coupled to the expectation values \bar{X}_i .

Up to this point, we have obtained $\frac{1}{2}N \times (N + 1) + N$ equations for all the variables. These equations provide some qualitative information about the

system. If we define $\bar{I}_{i+1} = \bar{X}_{i+1} - \bar{X}_i$, Eq. (21) can be cast into the form of a standard map,

$$\begin{aligned}\bar{I}_{i+1} &= \bar{I}_i + K_i \sin \bar{X}_i, \\ \bar{X}_{i+1} &= \bar{I}_{i+1} + \bar{X}_i.\end{aligned}\tag{27}$$

Similarly, if we define $Q_{i+1j} = G_{i+1j} - G_{ij}$, Eq.(25) can also be cast into the form of a map:

$$\begin{aligned}Q_{i+1j} &= Q_{ij} + [G(F - 2)]_{ij}, \\ G_{i+1j} &= G_{ij} + Q_{i+1j}.\end{aligned}\tag{28}$$

The difference between the classical case ($\tilde{\hbar} = 0$) and the quantum case is readily seen in Eq.(27) . In the classical case the coupling constant does not change from potential to potential; however, in the quantum case, the effective coupling constant changes from particle to particle. Because $G_{ii} > 0$ for any $\tilde{\hbar} \neq 0$, $K_i < K$, which implies that the quantum fluctuation will reduce the coupling strength. Another important difference is that in the classical case the positions of the particles in the ground state are determined by the standard map whereas in the quantum case they are determined by $(N + 1)$ -coupled two-dimensional maps. This makes the quantum FK model extremely difficult to study analytically.

One notices that when $\beta = 0$, $G_{ij} = 1/2$, which is the result of the coherent state theory. This is not the case in the quantum FK model. In Fig. 4 we plot $\tilde{\hbar}G_{ij}$ as a function of i and j . The data are obtained from QMC. It is obvious that $G_{ij} \neq 1/2$. Thus it seems that the coherent state is not adequate for the study of the quantum FK model.

We now make some comparisons with the QMC results. As mentioned before, to find the solution of these two sets of equations [Eqs.(21) and (25)] is equivalent to finding a periodic orbit in the $2(N + 1)$ -dimensional map [Eqs.(27) and (28)]. This is a very difficult problem to solve even numerically. Nevertheless, we will try to solve Eq.(21) self-consistently to see whether this equation can indeed give rise to the sawtooth map [5].

Using QMC, we obtained the expectation value of the particle's position \bar{X}_i , from which we can construct the quantum hull function f_q , as shown in Fig. 2(a) for $K = 0.5$ and (c) for $K = 5$, respectively. The quantum g_q -function is shown in Fig. 2(b) and (d) for $K = 0.5$ and $K = 5$, respectively. The quantum fluctuation $\tilde{\hbar}G_{ii}$ calculated from QMC is shown in Fig. 3 for the case $K = 5$.

As usual, we use Q particles and P external potentials with period 2π , and the

periodic boundary condition is imposed [14]: $\bar{X}_{Q+i} = \bar{X}_i + 2\pi P$. The results shown in the figure are for $P/Q = 34/55$.

To compare the squeezed state results with those from QMC, we substitute G_{ii} calculated from QMC into Eq.(21). We then compute the expectation value of the particles' positions by using Aubry's gradient method. We then construct the quantum hull function f_q and the quantum g_q -function shown in Fig. 5. The results agree surprisingly well with those from QMC. The most striking feature is the sawtooth shape of the g_q -function. This phenomenon was first observed by Borgonovi *et al.* [5] in their QMC computation and has been explained as a tunneling effect. Later, Berman *et al.* [6] obtained this result by using a mean field theory. In the framework of the squeezed state theory, the renormalization of the standard map to a sawtooth map is a consequence of quantum fluctuations. Our results show that the squeezed state approach indeed captures the effects of quantum fluctuations.

4 Quantum effects on the Aubry transition

In this section we will study the effects of quantum fluctuations on the Aubry transition. We will first study the behavior of the wave function of an incommensurate ground state. We will then introduce various indicators that might be used to characterize the quantum Aubry transition.

4.1 Ground state wave function of the quantum Frenkel-Kontorova model

We will use the QMC [15] to study the ground state of Hamiltonian (2). As in the classical case, we will concentrate our attention on the incommensurate state characterized by the golden mean winding number $\omega_G = (\sqrt{5} - 1)/2$. In the classical case the winding number is defined as the average separation of atoms per period, i.e., $\omega = \lim_{N \rightarrow \infty} \frac{X_N - X_0}{2N\pi}$. If ω is a rational number, the ground state is commensurate; and if it is an irrational number, the ground state is incommensurate. In the quantum case, \bar{X}_i is defined as the expectation value of the position of the i th particle. As usual, we use the method of continued fraction expansion and approximate ω_G by its rational convergents $\omega_n = F_n/F_{n+1}$, where F_n is the n th Fibonacci number defined by the recursion relation $F_{n+1} = F_n + F_{n-1}$ with $F_0 = 0, F_1 = 1$. In our computation, we choose F_{n+1} particles embedded in F_n external potentials.

Since the external potential is periodic with period 2π , we can fold the wave function to this period and then take the average over all the particles in the interval $[0, 2\pi]$. This quantity gives the probability of finding the particle at

a given position X . We plot the averaged probability density $\langle |\Psi|^2 \rangle$ in Fig. 6 with 144 particles embedded in 89 potentials for a fixed $\tilde{\hbar}$ ($= 0.2$) but different values of K . Here $\langle |\Psi|^2 \rangle$ is normalized, i.e., $\int_0^{2\pi} dX \langle |\Psi(X)|^2 \rangle = 1$. We observe that, in the small K regime, the probability of finding the particles at any point of the potential is almost the same (see, for example, the curve for $K = 0.1$). This is quite similar to the unpinned phase in the classical case. However, as the coupling constant increases, the probability of finding the particle in the upper part of the potential decreases whereas the probability of finding the particle in the lower part of the potential increases, as is noticeable from the appearance of peaks in the curves. As the coupling constant increases, the probability of finding the particles at the top is almost zero (see, for example, the curves for $K = 2$ and 5).

4.2 Indicators of the Aubry transition

4.2.1 Disorder Parameter

In the classical FK model, Coppersmith and Fisher [17] have proposed a “disorder parameter” to describe the transition from the pinned phase to the unpinned phase. This parameter is defined as the minimum distance of a particle from the top of the potential, $D = \min_{i,n} |X_i^e - 2\pi(n + \frac{1}{2})|$. If $D \neq 0$, the particles are pinned; when $D = 0$, they are unpinned. This “disorder parameter” also measures the discontinuity (or width of the biggest gap) of the hull function. One might want to use the same function to describe the quantum crossover. For instance, one may define a very similar quantum disorder parameter $D_q = \min_{i,n} |\bar{X}_i - 2\pi(n + \frac{1}{2})|$, where \bar{X}_i is the expectation value of the i th particle’s position. However, this parameter D_q could not capture the crossover of the ground state wave function. The reason is that, in the quantum case, the particle can tunnel from one side of the potential to the other. Thus the gap in the classical hull function does not survive quantum fluctuations (see Refs. [5] and [7]). It turns out that for large K , D_q might still be close to (or equal to) zero. Therefore, a new parameter is needed to describe the wave function crossover. To this end, we define the probability of finding the particles at the potential top as a quantum “disorder parameter”,

$$P_t = \frac{1}{N} \sum_{n=0}^{N-1} \int |\Psi(X)|^2 \delta \left[X - 2\pi(n + \frac{1}{2}) \right] dX. \quad (29)$$

In Figs. 7(a)-(b), we plot P_t as a function of K for different temperatures T_e ($T_e = \tilde{\hbar}/\tau$, where τ is the length of the imaginary time axis) and different system sizes. In Fig. 7(a), we fix $\tilde{\hbar}$ ($= 0.2$), $\omega = 13/21$ and set the temperature $T_e = 0.2/30, 0.2/120, 0.2/480$. The convergence is quite fast as is seen from the figure. The sharp decrease of P_t is very evident for $1 < K < 2$. In this small

K regime, P_t changes significantly: it drops almost two orders of magnitude. This drastic change can also be seen from Fig. 7(b). There the temperature is fixed at $T_e = 0.2/120$, which can be regarded as effectively zero temperature. The system size is changed from 21 particles to 144 particles.

4.2.2 Maximum Variance

Another parameter that can be used to depict this crossover is the maximal fluctuation of the particles. In the quantum case, we have observed that the particle situated at a position nearest to the top of the potential always has a maximal fluctuation since it has a higher classical potential energy. This observation has been verified numerically by QMC and theoretically by the squeezed state theory [7]. Thus we can use this maximal fluctuation as another measure of quantum “disorder”. To make a qualitative comparison with the classical disorder parameter D , we define

$$\Delta = \max_i \left[\sqrt{\langle (X_i - \bar{X}_i)^2 \rangle} \right]. \quad (30)$$

Here the average $\langle \dots \rangle$ is taken over all the paths (approximately 4,000) used in QMC. Δ as a function of K is plotted in Fig. 8. The computations given in this figure have been carried out with $\omega_n = F_n/F_{n+1} = 34/55$.

It is noticeable that the transition of the wave function is characterized by the different K -dependent behavior of Δ . In the small K regime, Δ is a constant independent of K but changes with $\tilde{\hbar}$. In the large K regime, Δ increases with K but does not change with $\tilde{\hbar}$. Furthermore, Δ is approximately equal to the classical disorder parameter D . For comparison, we have included D in the inset of Figure 8. In the classical case, the transition of course occurs at $K = K_c$.

These results show that the width and the shape of the probability density do not change with K in the small K regime. The width only depends on the strength of the quantum fluctuation $\tilde{\hbar}$. However, this picture changes significantly for large K . In this regime, the profile of the probability density spreads out, and the width of the probability density is quite insensitive to quantum fluctuations and depends only on the coupling constant. It should however be stressed that the analogy between D and Δ cannot be carried too far since Δ is not exactly the quantum correspondence of D . This is why even if we let $\tilde{\hbar}$ go to zero, Δ would not be zero in the small K regime.

4.2.3 Correlation function

As another indication of the quantum signature of the Aubry transition, we study the correlation function between the particles' fluctuations. The cross-correlation function C_{ij} is defined by

$$C_{ij} = \frac{l_{ij}}{\sqrt{l_{ii}l_{jj}}}. \quad (31)$$

It describes the fluctuation correlation between the particles i and j . $l_{ij} = \langle (X_i - \bar{X}_i)(X_j - \bar{X}_j) \rangle$ is the covariance of the fluctuations between the i th particle and the j th particle. Here $\langle \dots \rangle$ denotes the ensemble average over space and 'time' in QMC [14]. Since l_{ij} is symmetric, $C_{ij} = C_{ji}$. In our numerical calculations, we take 4000 paths and each path is divided into many steps in time, ranging from 1500 to 3000 depending on $\tilde{\hbar}$. The convergence is guaranteed by increasing the number of steps and the number of paths until the same results are reached.

Figure 9 shows the contour plots of C_{ij} for $K = 0.5$ and $K = 5$. The plots are drawn in 12 equal steps from -0.15 to 1 . A negative correlation function implies that the particles' quantum fluctuations are out of phase. The sharp change of C_{ij} from $K = 0.5$ to $K = 5$ is very readily noted. In the large K regime, the correlation function matrix C_{ij} is almost diagonal with a very small band width whereas in the small K regime the number of nonzero off-diagonal elements increases and the band width is much larger. Thus, in the small K regime, we have a much longer range interaction than in the large K regime. This can also be seen from the averaged correlation function $C(|i-j|) = \langle C_{ij} \rangle$, where $\langle \dots \rangle$ denotes the ensemble average over particles. We have investigated this function for a wide range of K . We tried to use different forms to best-fit this function, but found that it is very hard to see whether the decay is exponential, power-law or logarithmic. It seems that it obeys different laws in different ranges. Nevertheless, the correlation function in the large K regime decays faster than that in the small K regime, as illustrated in Fig. 10 for $K = 0.5$ and $K = 5$, respectively.

On the other hand, due to discreteness, it is also very difficult to define a parameter such as the width of the correlation function. As an alternative, we chose $C(1)$, which describes the correlation between the nearest-neighbor particles. In Fig. 11, we plot $C^{-1}(1)$ against K on a logarithmic scale. The signature of the transition is very similar to Fig. 8. In the small K regime, $C(1)$ is a constant (about 0.5); and in the large K regime, it decreases with K . Since the transition is largely smeared by quantum fluctuations, one can't define a critical K_c as in the classical case.

We know that if the correlation function decays exponentially in the short range, then $\ln C^{-1}(1) = l^{-1}$, which is just the Lyapunov exponent σ in the classical case [2], l being the correlation length. Thus, the parameter $C(1)$ captures the short-range correlation. Fig. 11 mimics the classical plot of the correlation length proposed by Aubry [2]. In the classical case, for $K < K_c$, $l = \infty$ and $\sigma = 0$, whereas for $K > K_c$, l is finite and $\sigma > 0$. However, in the quantum FK model, we do not have infinitely long interaction in the small K regime. Instead, we have a finite interaction range, but it is much longer than that in the large K regime.

5 Concluding remarks

The Frenkel-Kontorova model is a simple model. However, despite its deceptively simple appearance, it exhibits very complex behavior and contains very rich physics. It has found applications in a wide range of fields, from nonlinear dynamics to condensed matter physics to tribology. However, most of the studies have so far been confined to the classical Frenkel-Kontorova model. Very little work has been done on the quantum Frenkel-Kontorova model. We think this is indeed quite regrettable. The quantum Frenkel-Kontorova model is not only interesting from a theoretical point of view but is also important from a practical point of view. The work reported in this review represents only a first step in this direction. We however hope that it will serve as an impetus to further studies. It is our conviction that a thorough understanding of the quantum Frenkel-Kontorova model will lead to important breakthroughs both in theory and applications.

Acknowledgements

We would like to thank S. Aubry, F. Borgonovi, D. K. Campbell, H. Chen, R. B. Griffiths, C.-L. Ho, H.-Q. Lin, D. Shepelyansky, L.-H. Tang, and W.-M. Zhang for many helpful discussions. This work was supported in part by grants from the Hong Kong Research Grants Council (RGC) and the Hong Kong Baptist University Faculty Research Grant (FRG).

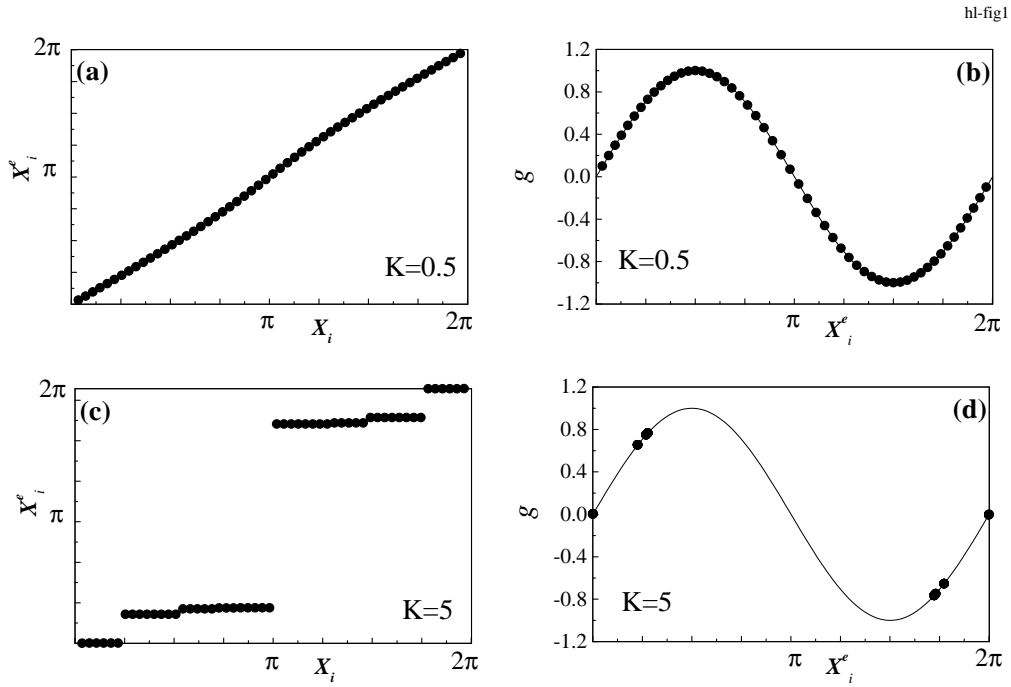


Fig. 1. The classical hull function and g -function in the subcritical regime ($K = 0.5$) and the supercritical regime ($K = 5$). In (b) and (d), the solid line is $\sin X^e$.

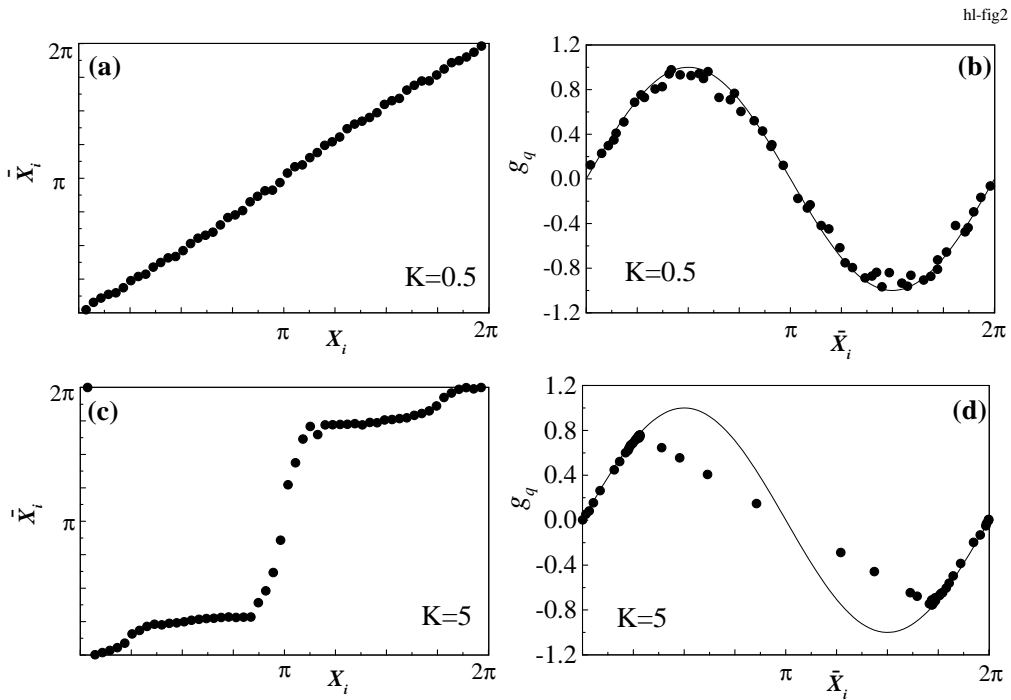


Fig. 2. The quantum hull function and g -function from QMC, $\tilde{\hbar} = 0.2$. The solid line in (b) and (d) is $\sin X$.

hl-fig3

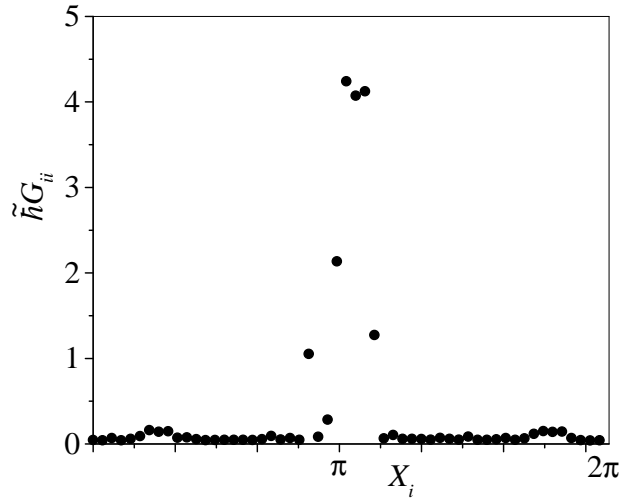


Fig. 3. $\Delta X_i^2 = \langle (X_i - \bar{X}_i)^2 \rangle = \tilde{h}G_{ii}$, calculated from QMC. The parameters are the same as in Fig. 2.

hl-fig4

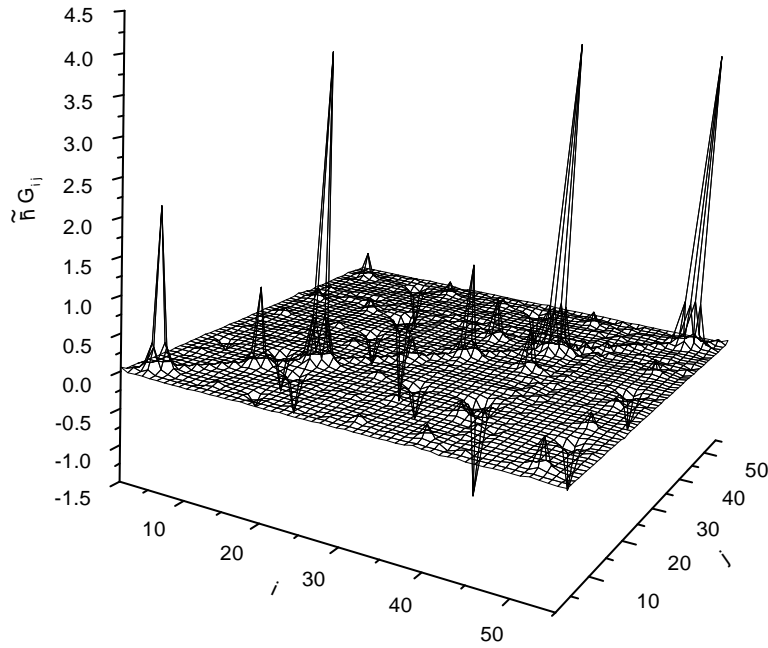


Fig. 4. $\tilde{h}G_{ij}$ as a function of i and j . The data are obtained from QMC with $\tilde{h} = 0.2$, $K = 5$.

References

- [1] Y. Frenkel and T. K. Kontorova, *Zh. Eksp. Teor. Fiz.* **8** (1938) 1340; F. Frank and J. van der Merwe, *Proc. R. Soc. London* **198** (1949) 205.

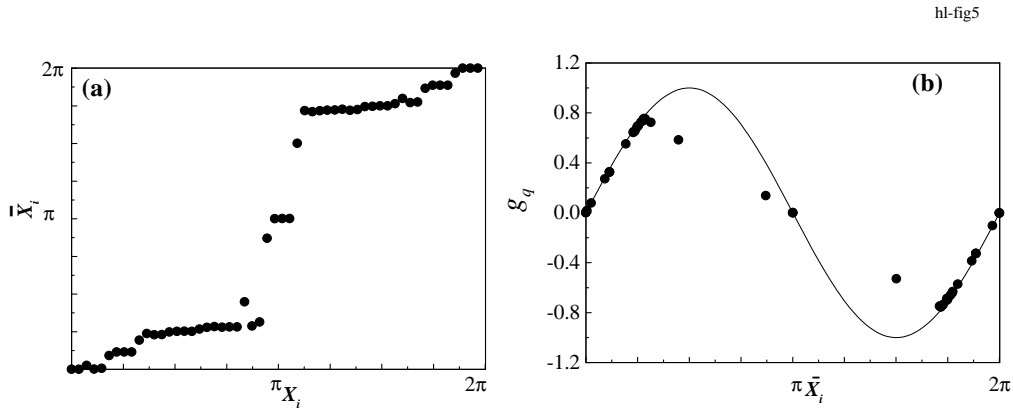


Fig. 5. The quantum hull function and g -function calculated from the squeezed state theory by substituting $\tilde{h}G_{ii}$ shown in Fig. 3 into Eq.(21).

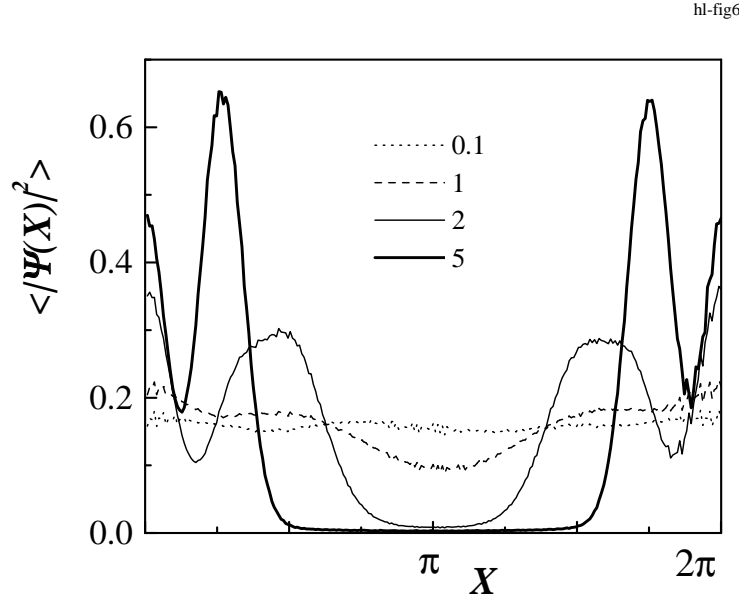


Fig. 6. The wave function of an incommensurate ground state with winding number $\omega_n = 89/144$ at fixed $\tilde{h} = 0.2$ for different values of K . $\langle |\Psi|^2 \rangle$ is the probability of finding the particle at X . The curves are for $K = 0.1, 1, 2$, and 5 , respectively. The wave function becomes localized in the lower part of the potential as K is increased to 2 and 5 .

- [2] S. Aubry, in *Solitons and Condensed Matter Physics*, edited by A. R. Bishop and T. Schneider. Springer-Verlag, Berlin 1978; *J. Phys. (Paris)* **44** (1983) 147; M. Peyrard and S. Aubry, *J. Phys. C* **16** (1983) 1593; S. Aubry, *Physica D* **7** (1983) 240; S. Aubry and P.Y. LeDaeron, *ibid* **8** (1983) 381.
- [3] M. G. Rozman, M. Urbakh, and J. Klafter, *Phys. Rev. Lett.* **77** (1996) 683; *Phys. Rev. E* **54**, (1996) 6485; M. Weiss and F. J. Elmer, *Phys. Rev. B* **53** (1996) 7539; T. Gyalog and H. Thomas, *Europhys. Lett.* **37** (1996) 195; O. M. Braun,

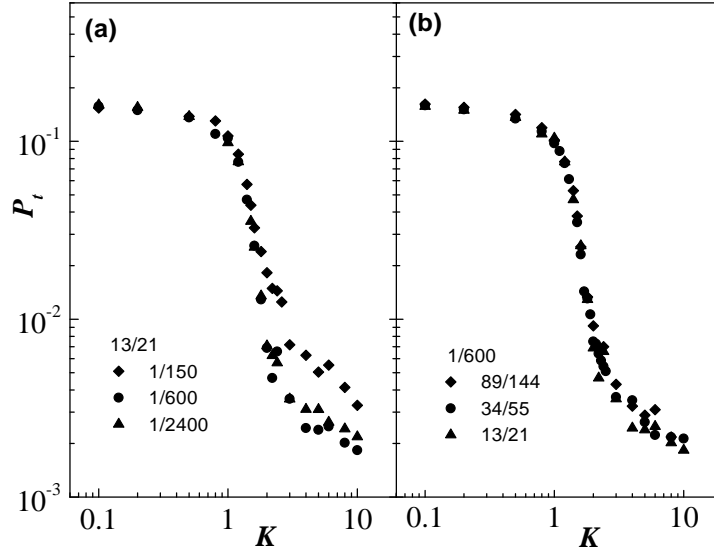


Fig. 7. The probability P_t of finding the particles at the top of the potential as a function of K for $\hbar = 0.2$. (a) P_t at temperatures $T_e = 0.2/30, 0.2/120$, and $0.2/480$ for $\omega_n = 13/21$. (b) P_t for $\omega_n = 13/21, 34/55$, and $89/144$ at a fixed temperature $T_e = 0.2/120$.

- T. Dauxois, M. V. Paliy, and M. Peyrard, *Phys. Rev. Lett.* **78** (1997) 1295, *Phys. Rev. E* **55** (1997) 3598; O. M. Braun, A. R. Bishop, and J. Röder, *Phys. Rev. Lett.* **79** (1997) 3692. T. Stunz and F. J Elmer, *Phys. Rev. E* **58** (1998) 1602, 1612.
- [4] M. G. Rozman, M. Urbakh, and J. Klafter, *Phys. Rev. Lett.* **77** (1996) 683; V. Zaloj, M. Urbakh, and J. Klafter, *Phys. Rev. Lett.* **81** (1998) 1227.
- [5] F. Borgonovi, I. Guarneri and D. Shepelyansky, *Phys. Rev. Lett.* **63** (1989) 2010; *ibid. Z. Phys. B* **79** (1990) 133, and F. Borgonovi, Ph.D dissertation, Università Degli Studi di Pavia, 1989, Italia.
- [6] G. P. Berman, E. N. Bulgakov and D. K. Campbell, *Phys. Rev. B* **49**, (1994) 8212.
- [7] B. Hu, *Quantum and Classical Correspondence: Proceedings of the 4th Drexel Symposium on Quantum Nonintegrability*, p. 445, eds. D. H. Feng and B. L. Hu. International Press (Cambridge, MA) 1997; B. Hu, B. Li, and W.-M. Zhang, *Phys. Rev. E* **58** (1998) R4068.
- [8] B. Hu and B. Li, *Europhys. Lett.* **46** (1999) 655.
- [9] W. M. Zhang, D. H. Feng and R. Gilmore, *Rev. Mod. Phys.* **62** (1990) 867; W. M. Zhang and D. H. Feng, *Phys. Rep.* **252** (1995) 1, and the references therein.
- [10] Y. Tsue and Y. Fujiwara, *Prog. Theor. Phys.* **86** (1991) 443, 469.

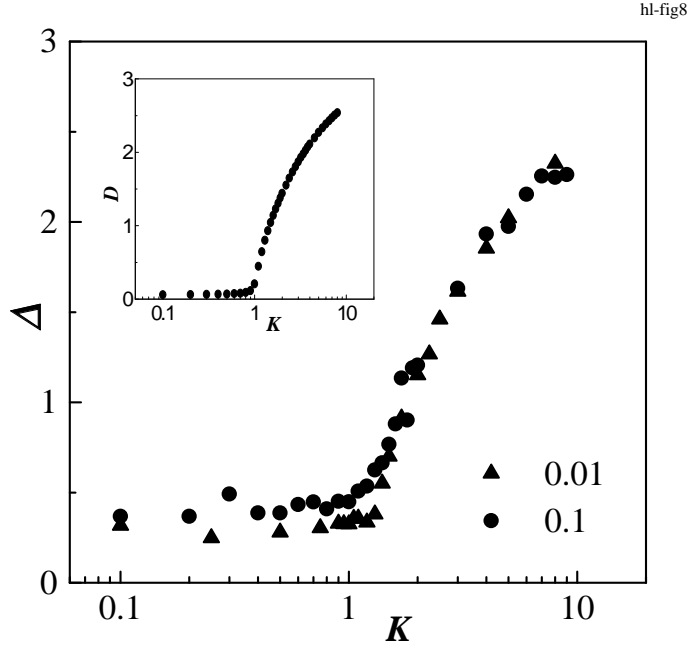


Fig. 8. The maximum variance Δ as a function of K for $\omega_n = 34/55$. Different symbols represent $\tilde{\hbar} = 0.01$ and 0.1 , respectively. We draw the classical disorder parameter D in the inset for comparison.

- [11] Y. Tsue, *Prog. Theor. Phys.* **88** (1992) 911.
- [12] A. K. Pattanayak and W. C. Schieve, *Phys. Rev. E* **56** (1997) 278.
- [13] B. Hu, B. Li, J. Liu, and J.-L. Zhou, *Phys. Rev. E* **58** (1998) 1743.
- [14] This is slightly different from that of Borgonovi *et al.* [5]. There they set $X_0 = 0, X_Q = 2\pi P$. We have calculated by QMC for both cases and found that the numerical results are slightly different. We use the periodic boundary condition.
- [15] M. Creutz and B. Freedman, *Ann. Phys.* **132** (1981) 472; E. V. Shuryak and O. V. Zhirov, *Nucl. Phys. B* **242** (1984) 393.
- [16] S. L. Sondhi, S. M. Girvin, J. P. Carini, and D. Shahar, *Rev. Mod. Phys.* **69** (1997) 315.
- [17] S. N. Coppersmith and D. S. Fisher *Phys. Rev. B* **28** (1983) 2566.

hl-fig9

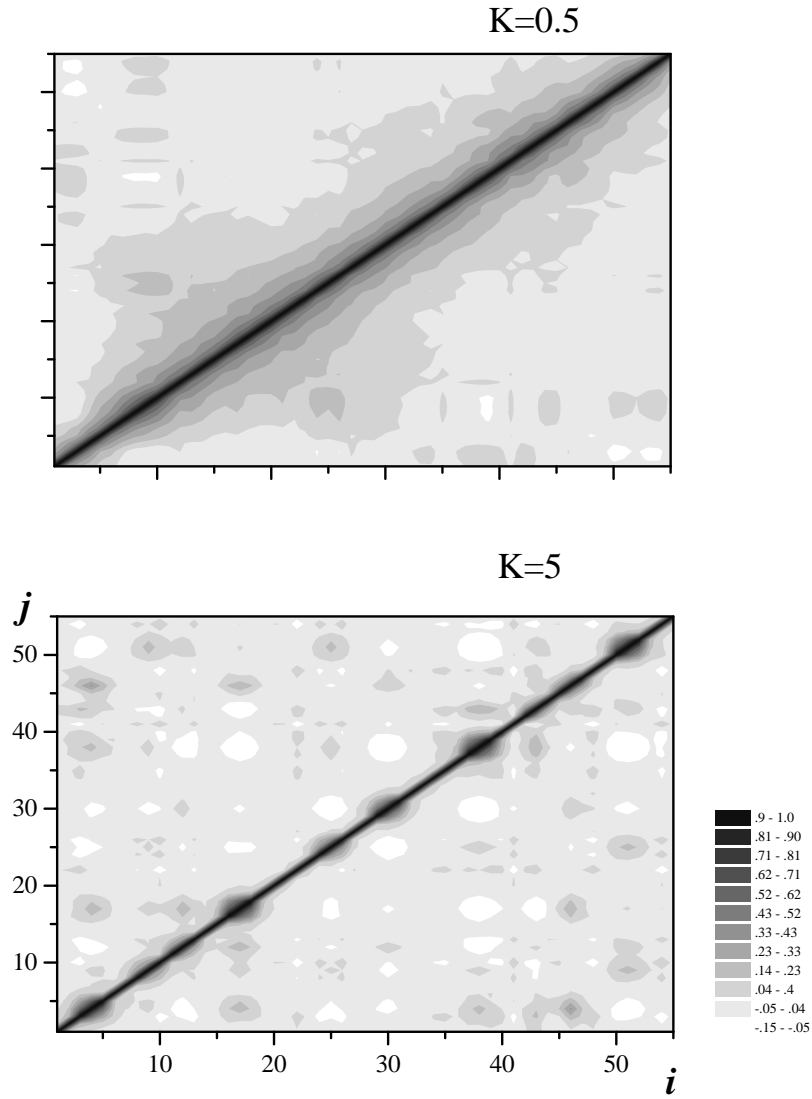


Fig. 9. Contour plot of the correlation function C_{ij} for $K = 0.5$ and $K = 5$ at $\tilde{h} = 1$.

hl-fig10

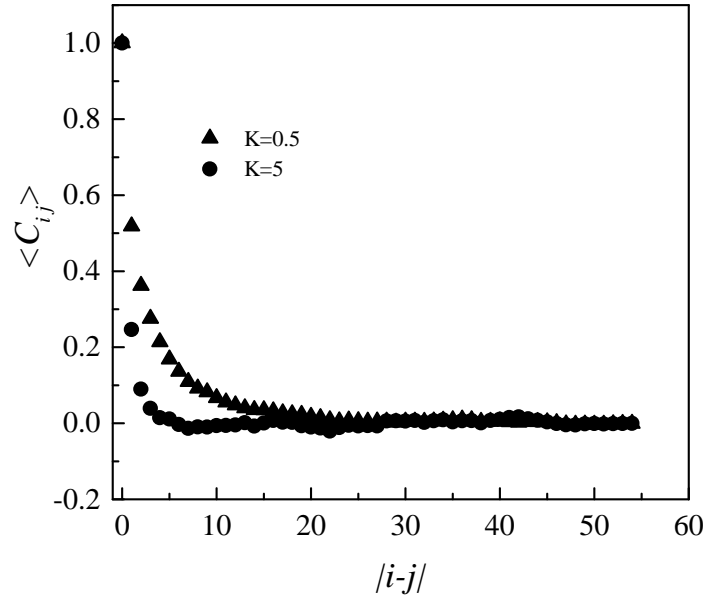


Fig. 10. $\langle C_{ij} \rangle$ as a function of $|i - j|$. The average is taken over the range of i and j , $\tilde{h} = 1$.

hl-fig11

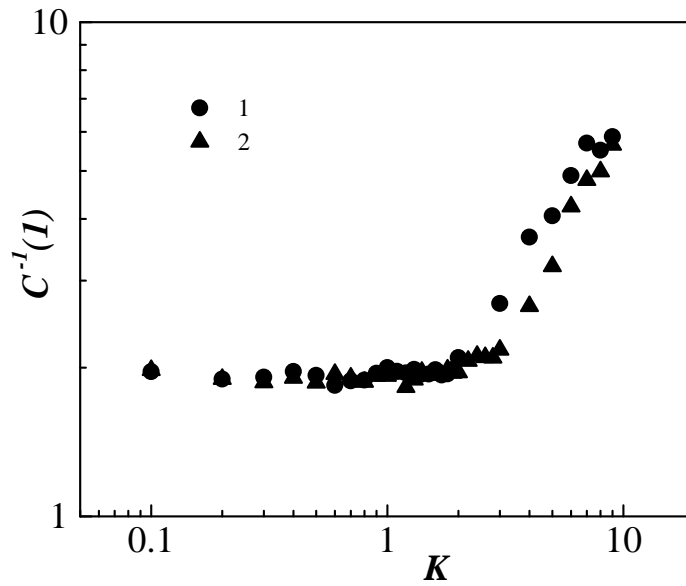


Fig. 11. $C^{-1}(1)$ as a function of K for $\tilde{h} = 1$ and 2, respectively.